Bioactive Materials 12 (2022) 278–291

Contents lists available at ScienceDirect

Bioactive Materials

journal homepage: www.keaipublishing.com/en/journals/bioactive-materials

DNA aptamer S11e recognizes fibrosarcoma and acts as a tumor suppressor

Yunyi Liu [a,1], Cheng Peng [a,1], Hui Zhang [c], Juan Li [a], Hailong Ou [a], Yang Sun [a], Chaoqi Wen [a], Dan Qi [d], Xiaoxiao Hu [a,b,**], Erxi Wu [d,e,f,*], Weihong Tan [a,c,g]

[a] State Key Laboratory of Chemo/Bio-Sensing and Chemometrics, College of Biology, College of Chemistry and Chemical Engineering, Molecular Science and Biomedicine Laboratory and Aptamer Engineering Center of Hunan Province, Hunan University, Changsha, Hunan, 410082, China
[b] Shenzhen Research Institute, Hunan University, Shenzhen, Guangdong, 518000, China
[c] Institute of Cancer and Basic Medicine, Chinese Academy of Sciences, The Cancer Hospital of the University of Chinese Academy of Sciences, Hangzhou, Zhejiang, 310022, China
[d] Department of Neurosurgery and Neuroscience Institute, Baylor Scott & White Health, Temple, TX, 76508, USA
[e] Texas A&M University Colleges of Medicine and Pharmacy, College Station, TX, 77843, USA
[f] LIVESTRONG Cancer Institutes and Department of Oncology, Dell Medical School, The University of Texas at Austin, Austin, TX, 78712, USA
[g] Institute of Molecular Medicine, Renji Hospital, Shanghai Jiao Tong University School of Medicine, And College of Chemistry and Chemical Engineering, Shanghai Jiao Tong University, Shanghai, 200240, China

ARTICLE INFO

Keywords:
Fibrosarcoma
Aptamer
Mitochondria
Apoptosis
Migration

ABSTRACT

Fibrosarcoma is a serious malignant mesenchymal tumor with strong invasiveness, high recurrence, and poor prognosis. Currently, surgical resection is the main treatment for fibrosarcoma. However, due to the lack of specific biomarkers, the inability to accurately diagnose fibrosarcoma can lead to sub-optimal surgical outcomes and decreased survival. Here, we seek to address this translational barrier and we show that DNA aptamer S11e was able to recognize fibrosarcoma cells (HT1080) but not human embryonic lung fibroblast cells with Kd values in the nanomolar range. In addition, we found that S11e discerned tumors in HT1080 xenograft mouse models and tumor tissues from fibrosarcoma patients. Furthermore, we demonstrated that S11e internalized into HT1080 cells independent of the lysosome pathway and located in mitochondria. Moreover, we revealed that S11e promoted the apoptosis of HT1080 cells and inhibited HT1080 cell migration. Finally, we investigated the biologically functional cellular target of S11e using a mass spectrometry approach, and identified that Diablo/SMAC protein is a cellular binding protein of S11e, by interacting to which S11e inhibited HT1080 cell migration and invasion. Taken together, these results provide the evidence that S11e may be useful for early diagnosis, targeted therapy, and prognostication of fibrosarcoma.

1. Introduction

In 2002, the World Health Organization (WHO) defined fibrosarcoma as a cancer consisting of fibroblasts and variable collagen [1]. Fibrosarcoma is a type of malignant neoplasm, originating from mesenchymal cells; it can occur in every part of human body with fibrous tissue and can occur at any age. Fibrosarcoma is mostly highly invasive and has a high recurrence rate. Lung is the most frequent site of fibrosarcoma metastasis, followed by the skeletal structure, lymph nodes, brain, and subcutaneous tissue [2]. Infant fibrosarcoma occurs in children under 5 years of age. Adult fibrosarcoma mostly occurs in adults aged 30–60 years, with a high degree of malignancy and prone to metastasis [3]. The incidence rate of fibrosarcoma in males and females is roughly equal. While surgical resection is the primary treatment, residual satellite lesions are the main cause of fibrosarcoma recurrence. However, multiple operations may lead to the progression of tumors. At present, fibrosarcoma lacks clinical pathological probes or biomarkers for its early stage [4]. Therefore, to potentially address this clinical need, it is important to explore the molecular probes or biomarkers for the early diagnosis, targeted therapy, and accurate prognosis of

Peer review under responsibility of KeAi Communications Co., Ltd.
** Corresponding author. State Key Laboratory of Chemo/Bio-Sensing and Chemometrics, College of biology, College of Chemistry and Chemical Engineering, Molecular Science and Biomedicine Laboratory and Aptamer Engineering Center of Hunan Province, Hunan University, Changsha, Hunan, 410082, China.
* Corresponding author. Department of Neurosurgery and Neuroscience Institute, Baylor Scott & White Health, Temple, TX, 76508, USA.
E-mail addresses: xxhu@hnu.edu.cn (X. Hu), erxi.wu@bswhealth.org (E. Wu).
[1] These authors contributed equally to this work.

https://doi.org/10.1016/j.bioactmat.2021.10.011
Received 4 February 2021; Received in revised form 2 September 2021; Accepted 6 October 2021
Available online 15 October 2021

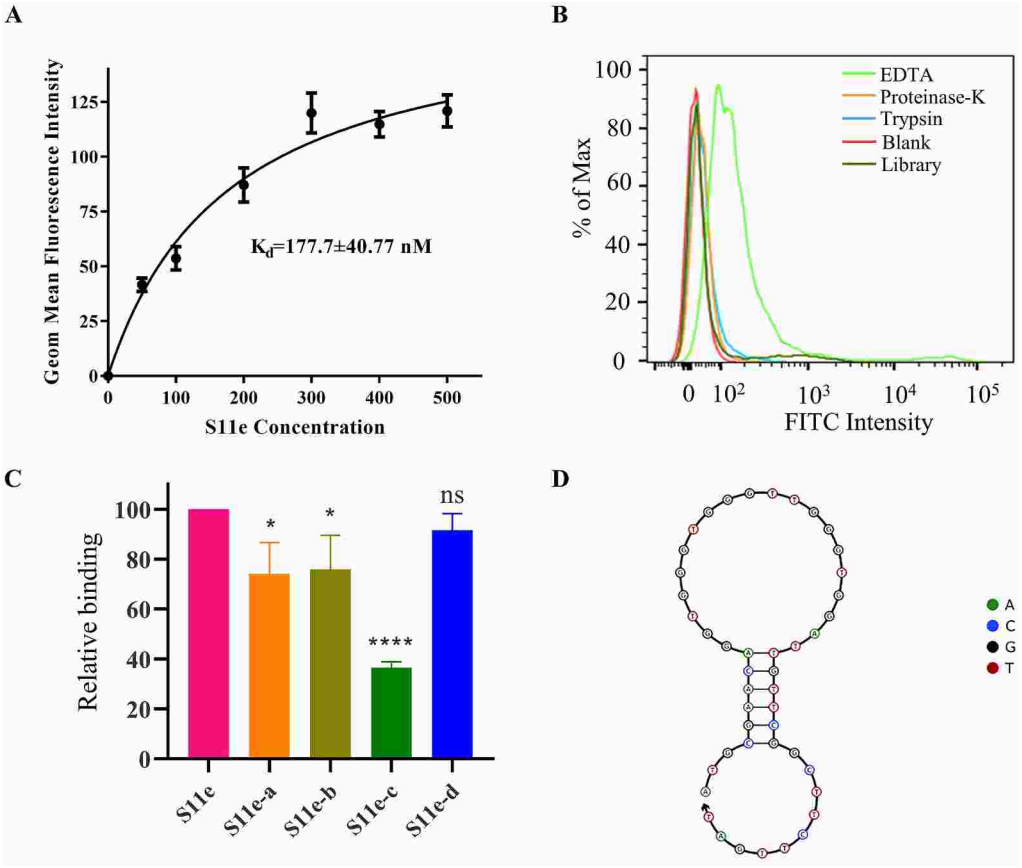

Fig. 1. Study on the characteristics of S11e. (A) The Kd of S11e for HT1080 cells was measured by flow cytometry. (B) After incubating with proteinase K, trypsin or EDTA, the binding of S11e to HT1080 cells was measured by flow cytometry. A Library with randomized aptamer sequences was used as a negative control (each sequence in this Library includes a randomized sequence region and two prime regions). Blank: unstained negative control. (C) Bar graph showing the binding of four truncated S11e sequences to HT1080 cells analyzed by flow cytometry. The quantified fluorescence intensities were shown by mean ± standard deviation calculated from multiple results. (Compared to full length S11e: $*p < 0.05$; $***p < 0.001$; *ns*, not significant). (D) S11e′s secondary structure was predicted by The Nucleic Acid Package (NUPACK).

fibrosarcoma patients.

Aptamers, which are usually screened by systematic evolution of ligands by exponential enrichment (SELEX), are single-stranded (ss) DNA or RNA sequences [5]. Aptamers are able to bind to specific targets with high affinity by forming a specific secondary or tertiary structure. Compared with antibodies, aptamers have good thermal stability, low immunogenicity, and high adaptability to a variety of targets, including peptides, proteins, cells, bacteria, etc. [6–8]. Aptamers have been studied in biomarker discovery, and anti-tumor drug delivery [9,10]. At present, 11 aptamers have entered the clinical trial stage, including pegaptanib, E10030, ARC1905, REG1, ARC1779, NU172, BAX499, AS1411, NOX-A12, and NOX-H94 [11–19]. Pegaptanib, which is the first aptamer drug and has been approved by The United States Food and Drug Administration (FDA), is used to treat age-related macular degeneration (AMD) [20]. REG1, ARC1779, NU172, and BAX499 are four aptamers for coagulation. AS1411 has been demonstrated to exhibit anti-tumor effects for a variety of cancer types, such as breast cancer, kidney cancer, and lung cancer [21,22]. NOX-A12 is another anti-tumor aptamer to treat chronic lymphoblastic leukemia, and multiple myeloma [18]. NOX-H94 and NOX-E36 are used to manage disease-induced inflammation [14,23].

Apoptosis is a conserved process of cell metabolism that plays a critical role in diseases. Apoptosis stimuli can lead to the release of several cell death inducers from the mitochondria, including cytochrome *c* and SMAC (also known as DIABLO). Cytochrome *c* promotes the formation of a cytosolic protein complex that activates an initiator caspase, caspase-9. Diablo/SMAC is a mitochondrial intermembrane protein, which is also an activator of caspase [24]. They have a short region of similarity at their N-termini through which they can interact with inhibitors of apoptosis (IAP) proteins, and antagonizing IAP inhibition of caspases to promote cell death, as well as affect tumor cell cycle and other pathways in cancer, which show that Diablo/SMAC may be an important player and potential therapeutic target in tumor therapy.

In order to solve the current problems of cell-SELEX, we have applied a non-selective strategy to obtain an aptamer S11e to specifically recognize fibrosarcoma cells. Our work provides compelling evidence that S11e is a promising tool for fibrosarcoma diagnosis and therapy and opens the door as a paradigm for developing new strategies for fibrosarcoma therapy.

2. Materials and methods

2.1. Aptamer synthesis and labeling

All of the ssDNA aptamers appeared in the experiments were synthesized and labeled by Sangon Biological Technology Co., Ltd (Shanghai, China) and Hippo Biological Technology Co. Ltd (Huzhou, China).

2.2. Cell culture

Cell lines were cultured in sterile environment containing 5% CO_2 at 37 °C. HT1080 (Fibrosarcoma cells) (CAS, cell bank Shanghai, China) and MRC-5 (Human embryonic lung fibroblast cell) (CAS) were cultured in MEM medium supplemented with 10% fetal bovine serum (FBS). U-2 OS (Osteosarcoma cells) (CAS) cells were cultured in McCoy's 5a Medium Modified supplemented with 10% FBS.

2.3. Aptamer binding detection

Washing buffer (WB) was Dulbecco's phosphate buffered saline (D-PBS) mixed with 5 mM $MgCl_2$ and 4.5 g/L glucose. Then, 0.1 mg/mL yeast tRNA and 1 mg/L BSA were added into the WB to form the binding buffer (BB).

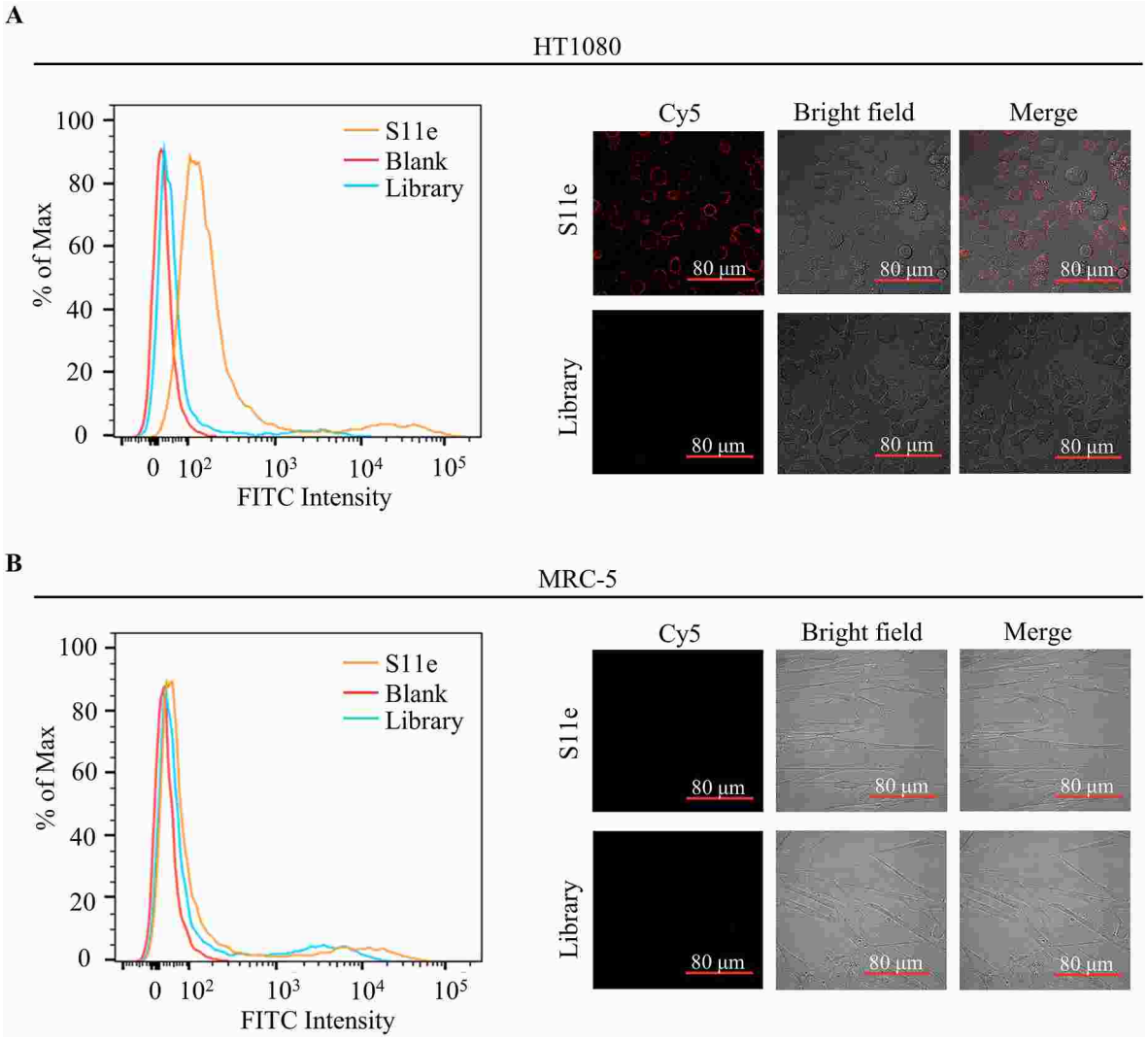

Fig. 2. Identification of a DNA aptamer that can specifically bind to fibrosarcoma cells. (A) HT1080 cells were incubated with FITC-labeled S11e at 4 °C, the binding ability was analyzed by flow cytometry. The Cy5-labeled S11e (250 nM) binding to HT1080 cells was displayed by confocal microscopy, and Library: randomized sequences used as a control. Blank: unstained negative control. (B) Similarly, the ability of S11e binding to MRC-5 was monitored by flow cytometry at 4 °C. Images were captured by confocal microscopy.

HT1080 or MRC-5 cells were cultured in 75-mm cell dishes. When the cell density reached 90%, cells were washed with D-PBS and digested with 0.2% EDTA. 3×10^5 cells were collected in a 1.5 mL Eppendorf (EP) tube and incubated with 250 nM FITC-labeled ssDNAs in BB for 1 h. Samples were washed with WB and the fluorescence signals were detected by BD FACSVerse™ Flow Cytometer (BD Biosciences, USA). All experiments in this study were repeated three times.

2.4. Confocal microscopy imaging

Cells were cultured in optical dishes (NEST Biological Technology Co., Ltd, China) for 24 h. Then, the cells were incubated with Cy5-labeled aptamers for 1 h. Before further assays, cells were washed several times with WB. The binding of aptamers to cells was monitored by confocal microscopy (Zeiss LSM510) and images were analyzed using FV10-ASW version 3.1 software. All experiments were repeated three times.

2.5. Target type determination

HT1080 cells were cultured in 35-mm cell dishes. After culturing and reaching a density of 90%, the cells were washed with WB. Then, 200 μL of 0.1 mg/mL of proteinase K or 0.25% trypsin was added for 1 min, and the complete medium was added to terminate the digestion. These cells were pipetted with WB and centrifuged at 1200 rpm for 4 min, and incubated for 1 h at 4 °C after 250 nM FITC-labeled aptamers were added. After the incubation, these cells were washed with WB and the fluorescence signals were detected by flow cytometry. The experiments were repeated three times.

2.6. Affinity analysis

The affinity analysis was conducted following the previously reported methods [25]. 3×10^5 HT1080 cells were incubated with a concentration gradient of FITC-labeled aptamers or Library at 4 °C for 1 h. The fluorescence intensity was tested by flow cytometry. The average fluorescence intensity was subtracted from that of the cells incubated with Library, and the curve of Kd was obtained from the equation of $Y = B_{max}\ X/(Kd + X)$ (Y: relative fluorescence intensity; X: aptamer concentration). Finally, results were plotted with Graph Pad Prism 7.0. All experiments were repeated three times.

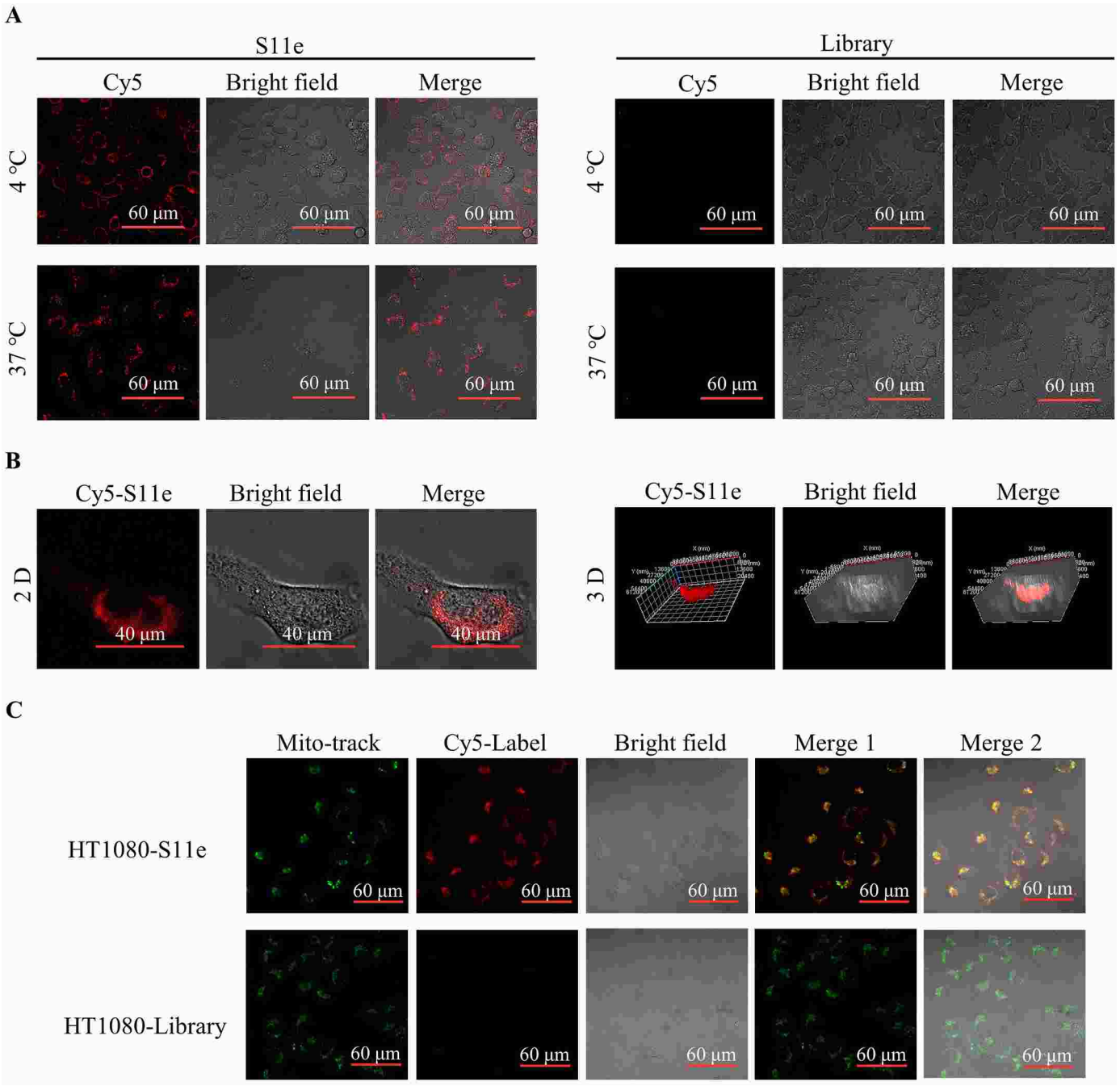

Fig. 3. Internalization of S11e in HT1080 cells. (A) HT1080 cells were incubated with Cy5-labeled S11e at 4 °C or 37 °C, then images were captured by confocal microscopy. (B) After incubating with Cy5-labeled S11e at 37 °C, the two-dimensional (2D) and three-dimensional (3D) images were captured by confocal microscopy. (C) Co-localization of the Cy5-S11e (red) and Mito-tracker (green).

2.7. Colocalization experiment

HT1080 cells were seeded into a 35-mm optical vessel. After incubation at 37 °C for 24 h, 500 μL of Cy5-labeled aptamer was appended at a total concentration of 250 nM. After incubation for 1 h, the supernatant was removed and 500 μL of Mito-tracker (C1048, Beyotime) solution or lysosome-tracker (C1046, Beyotime) was added at a final concentration of 200 nM at 37 °C for 30 min. Fluorescence signals were detected by Zeiss LSM510. All experiments were repeated three times.

2.8. In vivo fluorescence imaging

5–6 weeks old male athymic BALB/c (BALB/c-nude) mice were purchased from Hunan SLAC Experimental Animal Co., Ltd. 5×10^6 HT1080 cells were injected subcutaneously into the back of nude mice. As soon as the tumor volume reached a diameter of 1.0 cm, 100 μL phosphorothioate (PS) modified Cy5-S11e (Cy5-S11e-PS) or PS modified Cy5-Library (Cy5-Library-PS) was injected into mice *via* tail vein, and the final concentration was 5.5 μM. At 5 min, 30 min, 1 h, 2 h, 3 h, fluorescent images were collected by the *In vivo* Imaging System (IVIS) Lumina II imaging system (Caliper Life Science, USA). After fluorescence imaging analysis, tumor-bearing mice injected with Cy5-S11e-PS or Cy5-Library-PS were sacrificed and dissected. Tumor tissue and visceral organs including spleen, kidneys, liver, heart and lung were then imaged. All animal experiments were performed in compliance with the regulations of Institutional Animal Care and Use and were approved by

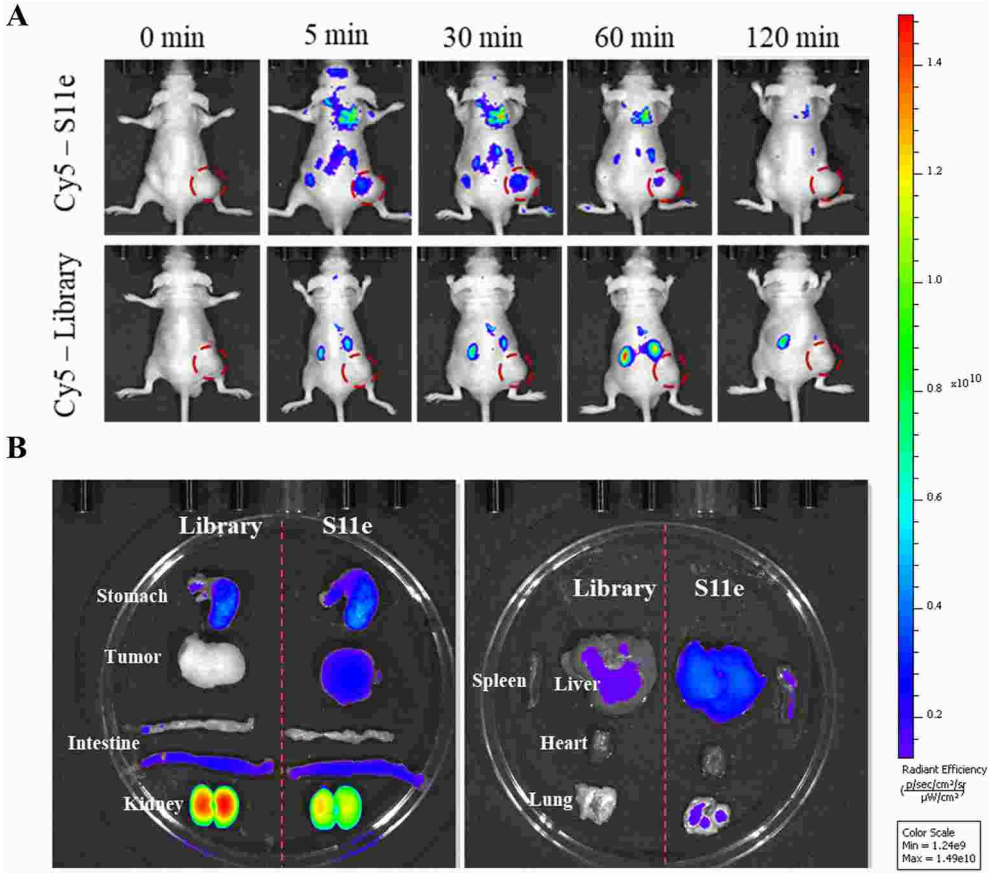

Fig. 4. Fluorescence Imaging of S11e in xenografted mouse models. (A) Fibrosarcoma tumor-bearing mice were intravenously injected with Cy5-labeled S11e (upper panel) or Cy5-labeled randomized Library (lower panel). Fluorescence images were taken by *in vivo* imaging system. (B) Optical and fluorescent images of organs isolated from fibrosarcoma tumor-bearing mice at 30 min after injection.

Hunan Experimental Animal Center. The mice experiments were repeated three times.

2.9. Human tissue microarray staining

The slides of fibrosarcoma tissue array (SO2084) were purchased from Xi'an Elina Biotechnology Co., Ltd. These slides were preheated at 60 °C for 30 min and then immersed in xylene for 30 min. They were sequentially immersed in a gradually decreasing ethanol solution for rehydration (100%, 95%, 90%, 80%, and 70%) at 5 min intervals. They were washed with WB, and placed in 0.01 M citrate (pH 6.0), heat for 20 min. After naturally cooled down at room temperature, they were treated with pre-cooled blocking buffer (BB, 20% FBS and 0.1 mg/mL salmon sperm DNA) for 1 h. They were then incubated with 250 nM Cy5-labeled aptamer S11e and Library for 1 h at 4 °C, separately. Finally, the fluorescence images were captured by a Panoramic SCAN (3DHISTECH, Spain). Fluorescence intensity was calculated and marked as negative (–, <30,000), weak (+, 30,000–60000), moderate (++, 60,000–100000) or strong (+++, >100,000), respectively.

2.10. Cytotoxicity assay

Cells were seeded in 96-well plates at 5000 cells/well. After the cells were attached, a concentration gradient of Library or S11e was added and cultured at 37 °C for 24 h, 48 h, and 72 h, respectively. After supernatant removal, these wells were washed with D-PBS and then CCK-8 solution was added. After incubating at 37 °C for 1 h, the plates were then detected by Microplate Reader Synergy 2 (BioTek, USA). All experiments were repeated three times.

2.11. Scarification test

HT1080 cells were seeded into 6-well plates for 24 h. Then, the cells in monolayer were vertically scratched. The floating cells were removed by D-PBS and cultured at 37 °C with 8 μM Library or S11e. Images were taken daily through an inverted microscope (EVOS f1, AMG Corporation, USA).

2.12. Transwell assay

HT1080 were seeded into 24-well plates, then 5 μM ssDNA was added and incubated with the cells for 0 h, 12 h, and 24 h. Transwell chamber (Merck Millipore Ltd, MCEP24H48) was placed in a new 24-well plate, and then solidified in an incubator for 4 h after Matrigel addition. 2×10^4 aptamer-treated cells were added into the chamber (200 μL cell suspension + 800 μL complete medium), and cultured for another 24 h. Cells were then fixed with 95% ethanol for 20 min and stained with Giemsa for 10 min. Resulting cells were photographed under an inverted microscope (EVOS f1, AMG Corporation, USA).

2.13. Western blotting

HT1080 cells were seeded in 75-mm dishes and incubated for 24 h. When the cells reached 70–80% confluency, they were washed with D-PBS and harvested by centrifugation. Then, the RIPA buffer (P0013B, Beyotime) with Protease Inhibitor Cocktail (4,693,159,001, Roche) was added to lyse cells. Proteins were separated using 10% SDS polyacrylamide gels (P2012, NCM Biological Technology Co. Ltd) and transferred to PVDF membranes (Merck Millipore Ltd, ISEQ00010).

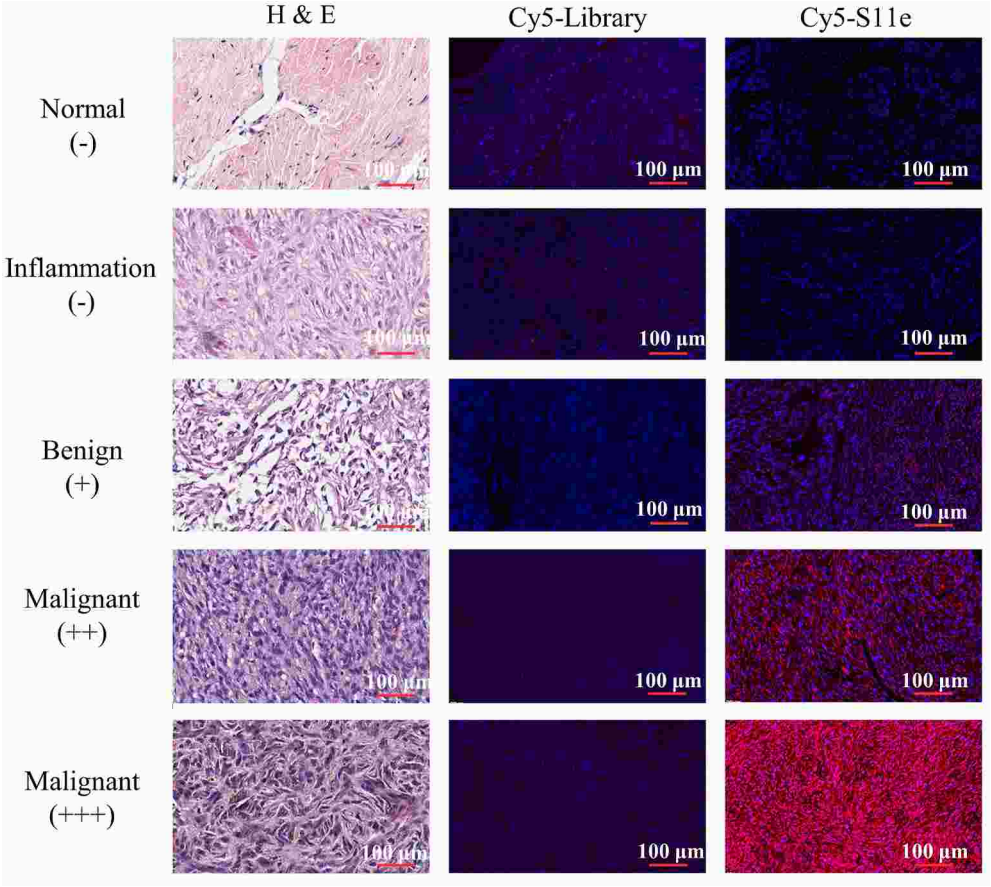

Fig. 5. S11e recognizes tumor cells in patient tissue samples. Fibrosarcoma tissue array were incubated with Cy5-labeled S11e or randomized Library. Fluorescence signals were detected with Panoramic scan.

Membranes were then incubated with primary antibodies at 4 °C overnight. The followings are the antibodies used in this study: anti-poly (ADP-ribose) polymerase (PARP) antibody (A19596, Company ABclonal Inc.), *anti*-caspase-3 antibody (sc-56053, Santa Cruz Biotechnology), *anti*-caspase-9 (sc-56076, Santa Cruz Biotechnology) antibody, *anti*-Diablo/SMAC antibody (AF789-SP, Santa Cruz Biotechnology). After washing three times with Tris-buffered saline with 0.1% Tween 20 (TBST), goat anti-rabbit secondary antibody (A9169, Sigma) was added to the membrane. The signal was detected with WesternBright™ ECL (K-12045-D50, Advansta) and visualized by ChemiDoc™ XRS Imager (Bio-Rad, USA).

2.14. Apoptosis assay

1×10^5 HT1080 cells were cultivated in a 35-mm dish, and unlabeled S11e was added to the cells. After 72 h incubation at 37 °C, the supernatant was transferred to a 15 mL centrifuge tube. Cells were treated with EDTA-free trypsin and transferred to the same centrifuge tube. After centrifuged at 1300 rpm for 5 min. Cell apoptosis was analyzed using Annexin V-FITC (C1062 M, Beyotime) according to the manufacturer's protocol. Fluorescent signals were detected by flow cytometry. Apoptosis assay was repeated three times.

2.15. Mass spectrometry (MS) analysis

Because the modification of biotin at the 5-terminal of S11e may decrease its binding efficiency, we used flow cytometry to test the binding ability of biotin-modified S11e to HT1080 cells. The result showed that biotin-modified aptamer could still bind HT1080 cells with high affinity. Next, HT1080 cells were washed three times with pre-cooled PBS buffer and incubated with 400 nM biotin-modified S11e or biotin-modified Library in 4 mL of BB containing protease inhibitors (0.1 mM PMSF) at 37 °C for 1 h. After incubation, the plasma membrane proteins of the HT 1080 cells were isolated by SM-005 Minute Plasma Membrane Protein Isolation and Cell Fractionation Kit (Invent biotech corporation, USA). Subsequently, the protein-Library or protein-S11e complex was captured by incubating with 2 mg (200 μL) of streptavidin beads at 4 °C for 45 min. After a collection by centrifugation, the proteins were eluted by heating in 30 μL of loading buffer and analyzed by SDS- PAGE gel and silver staining. The aptamer-purified protein bands were excised for digestion in situ and analyzed by liquid chromatography (LC)-MS/MS (APTBIO Co., Ltd, China).

2.16. Aptamer-based pull-down assay

The protein samples were prepared in the same manner as described for MS analysis. The captured proteins mixed with 40 μL of protein loading buffer (2 ×). The solution was heated at 95 °C for 5 min to denature the proteins. After centrifugation at 5500 rpm, 4 °C for 5 min, the solution was subjected to 12% SDS-page gel electrophoresis. Then, the gels were stained with Silver Stain Kit (Beyotime, Biotech P0017S) and scanned using a gel imaging system (Microtek, Bio-6000).

2.17. Lentivirus-mediated RNA interference

Lentivirus particles harboring a short hairpin RNA (shRNA) targeting Diablo/SMAC (shRNA1, 5'-GATCCGCGTTG ATTGAAGCTATTACTTTCAAGAGAAGTAATAGCTTCAATCAACGCT TTTTTA-3'; shRNA2, 5'-GATCCGCGCAGATCAGGCCTCTATA ATTCAAGAGATTATAGAGGCCTGATCTGCGCTTTTTTA-3'; shRNA3

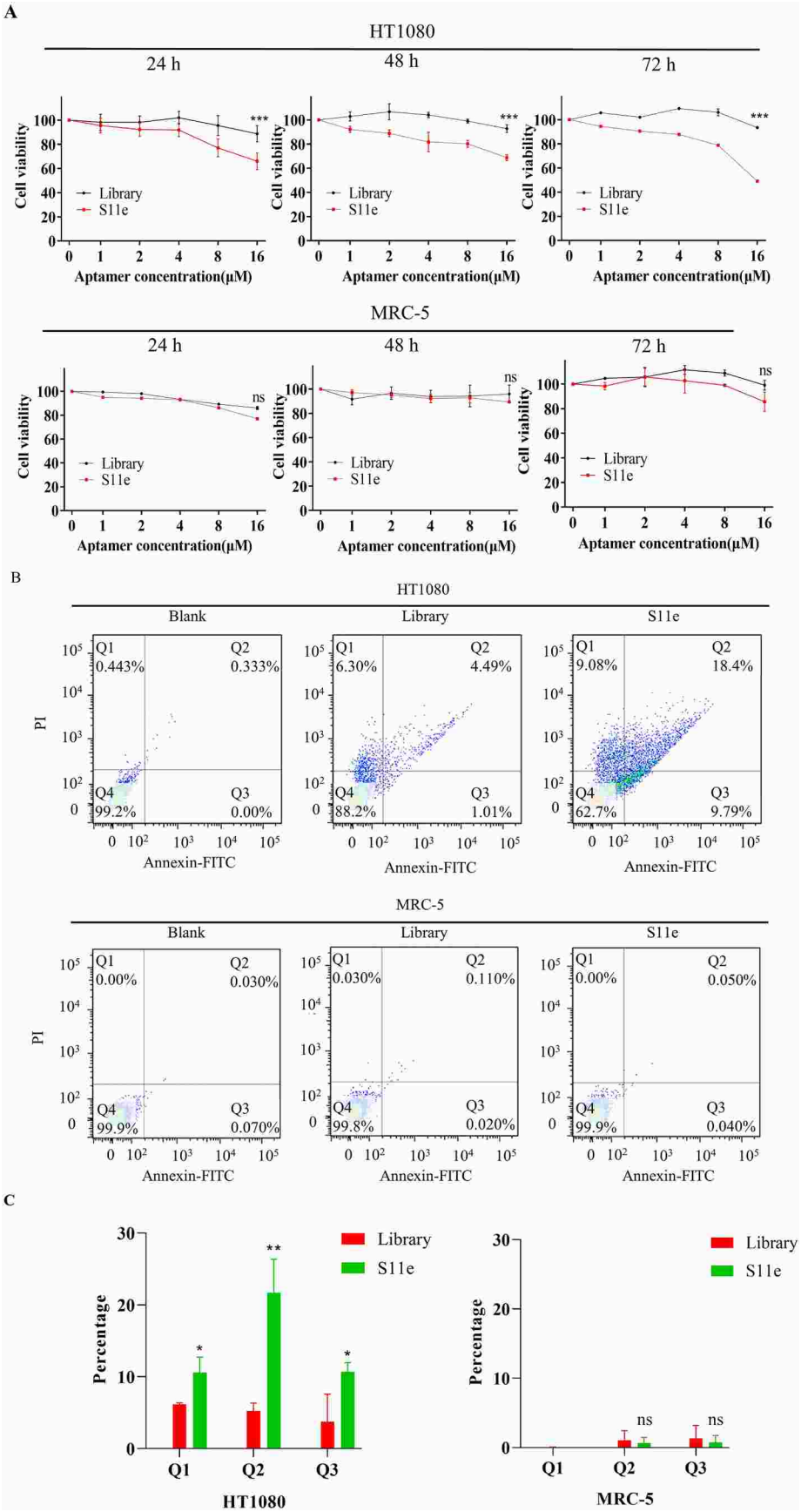

Fig. 6. S11e promotes apoptosis of fibrosarcoma cells. (A) HT1080 and MRC-5 cells were incubated with the indicated 16 μM concentrations of S11e or randomized Library. After adding CCK-8, the cytotoxicity of 24 h, 48 h, and 72 h treatment was detected by microplate reader (Comparison, S11e vs Library: ***$p < 0.001$; *ns*, not significant). (B) Detection of apoptotic effects of aptamers on HT1080 cells and MRC-5 cells by flow cytometry. (C) Statistical evaluation of apoptotic flow cytometry results (Comparison, S11e vs Library: *$p < 0.05$; **$p < 0.01$; *ns*, not significant).

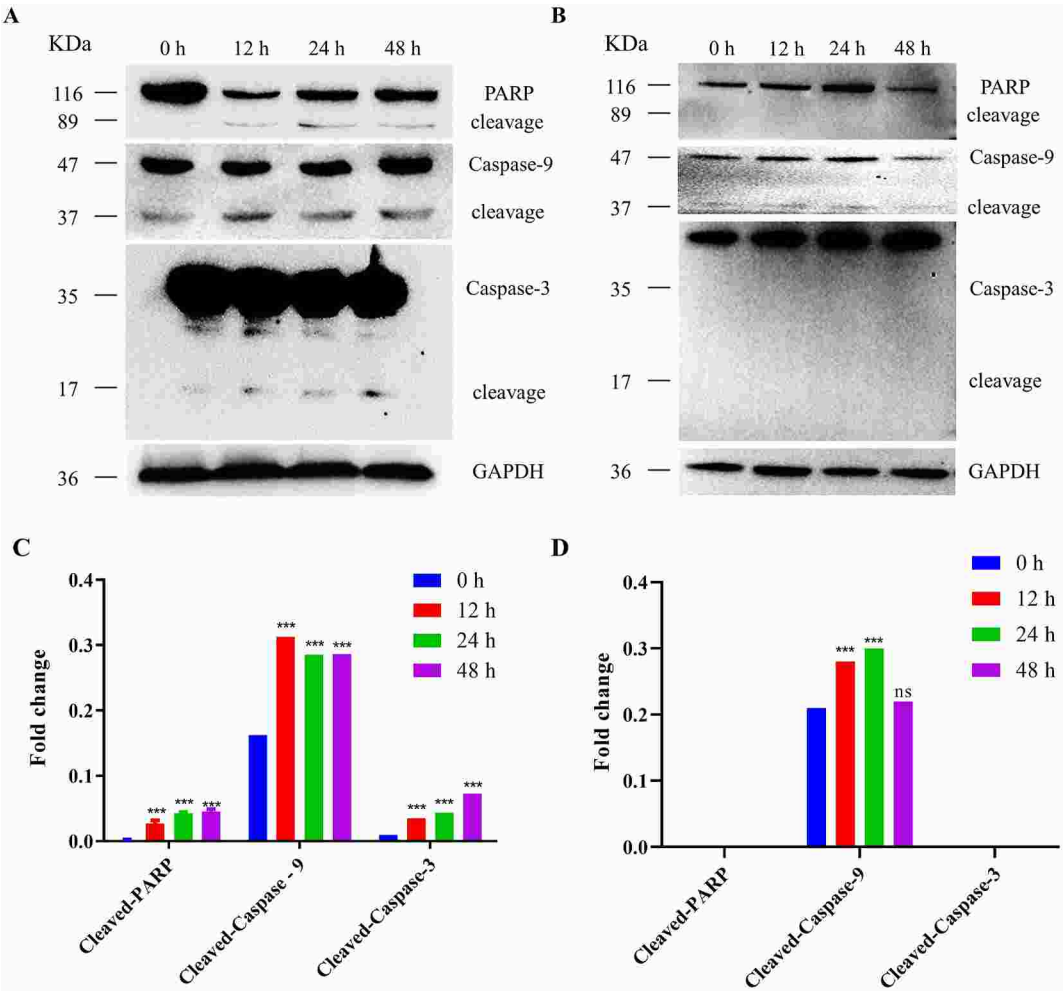

Fig. 7. S11e regulates mitochondrial-mediated endogenous apoptotic pathway in HT1080 cells. Western blotting was used to analyze the expression of cleaved-PARP, cleaved-Caspase-9 and cleaved– Caspase-3 in HT1080 cells treated with S11e (A) or Library (B) for 0 h, 12 h, 24 h, 48 h. Quantified data of Western blotting results in An under treatment by S11e (C) and Library (D) were analyzed statistically (Compared to 0 h: ***$p < 0.001$; *ns*, not significant).

5'-GATCCGCTGGCAGAAGCACAGATAGATTCAAGA-GATCTATCTGTGCTTCTGCCAGCTTTTTTA-3') or a scramble negative control shRNA (5'-GATCCGCGGCTTTTTTA-3'), were purchased from Vigene Biosciences (Jinan, China). HT1080 cells were incubated with lentivirus particles for 24 h and subsequent selection was performed with puromycin treatment for 4 days.

2.18. Statistical analysis

All statistical analyses were conducted with Graph Pad Prism 7.0. Statistical significance analyses were performed with the t tests and $p < 0.05$ was deemed significant.

3. Results

3.1. Identification of ssDNA aptamers against fibrosarcoma cells HT1080

Aptamers are generally obtained by time-consuming SELEX, with multiple rounds of screening and analysis. We here used our previously found aptamers with known sequences as a pool for our non-SELEX strategies (The sequences are listed in Table S1). The binding abilities of all aptamers in this pool to HT1080 cells were tested by flow cytometry. As a result, we successfully identified an aptamer S11e [26] that can bind to HT1080 cells (Fig. S1). We found that the equilibrium dissociation constant (Kd) was 177.7 ± 40.77 nM, indicating its high affinity for HT1080 cells (Fig. 1A). To determine which type of target molecule S11e binds to, HT1080 cells were treated with 0.2% EDTA, proteinase K or trypsin, respectively, and then incubated with S11e at 4 °C for 1 h. The fluorescence intensity was measured by flow cytometry. The result showed that the affinity of S11e binding to HT1080 cells decreased after treated with proteinase K or trypsin, 0.2% EDTA was used as control (Fig. 1B), suggesting that the S11e targeting molecule may be a protein.

3.2. Sequence optimization

The aptamers with fewer nucleotides, i.e., truncated aptamers, are more cost-efficient for chemical synthesis. They may have higher tissue permeability and lower immunogenicity than their original forms [27]. As shown in Table S2, four truncated sequences of S11e-a, S11e-b, S11e-c, and S11e-d were synthesized by deleting 5′ and 3′ bases of the aptamer S11e (45 nt, 1–45). The individual binding of each shortened aptamer to HT1080 cells was detected by flow cytometry. S11e-a (4–35 nt), S11e-b (4–30 nt) and S11e-d (6–30 nt) partially retained their ability to bind HT1080 cells, while S11e-c (4–22 nt) lost the ability (Fig. 1C).

The specificity of aptamers binding to tumor cells is a prerequisite for the potential clinical application. We tested the binding selectivity of S11e to HT1080 cells and MRC-5 cells (a negative control), respectively. These cells were treated with FITC-labeled S11e at 4 °C for 1 h and fluorescence intensity was detected by flow cytometry (Fig. 2A and B).

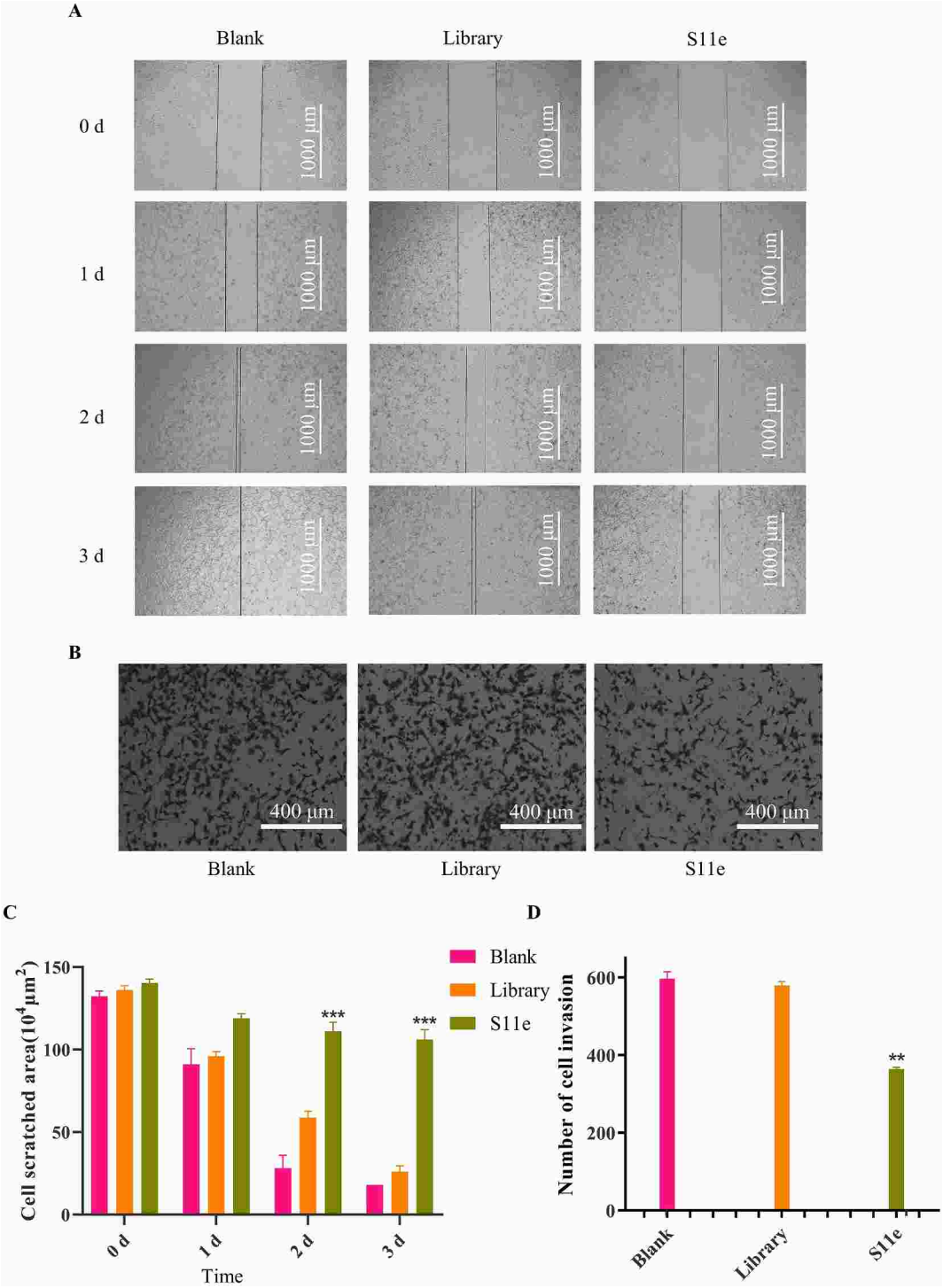

Fig. 8. S11e inhibits the migration and invasion of HT1080 cells. (A) The cell migration was monitored for 3 days, the representative images captured by an inverted microscope were shown here. (B) The number of invasive cells in a transwell chamber after treatment with S11e and Library for 24 h was observed by an inverted microscope. The representative images were shown here. (C) Statistically analyzed data of A (Comparison, S11e vs Library: $^{***}p < 0.001$). (D) Statistically analyzed data of B (Comparison, S11e vs Library: $^{**}p < 0.01$; $^{***}p < 0.001$).

The result showed that S11e binds to HT1080 cells but not MRC-5 cells (Fig. S3). Confocal images of HT1080 cells and MRC-5 cells incubated with Cy5-labeled S11e further demonstrated that S11e only binds to HT1080 cells, suggesting its binding selectivity to tumor cells (Fig. 2B).

3.3. Internalization and intracellular localization

To address the cellular localization of S11e after binding to fibrosarcoma cells, we conducted confocal experiment. HT1080 cells were treated with Cy5-labeled S11e for 1 h at 4 °C or 37 °C, respectively. The results showed that the fluorescence signals of S11e mainly appeared on the cell membrane at 4 °C, while most of the fluorescent signals of S11e were in the cytoplasm at 37 °C (Fig. 3A). It was further confirmed with the three-dimensional (3D) image captured by confocal Z-axis scanning (Fig. 3B). In contrast, no fluorescent signals were detected in MRC-5 cells at either 4 °C or 37 °C (Fig. S2). Together, these

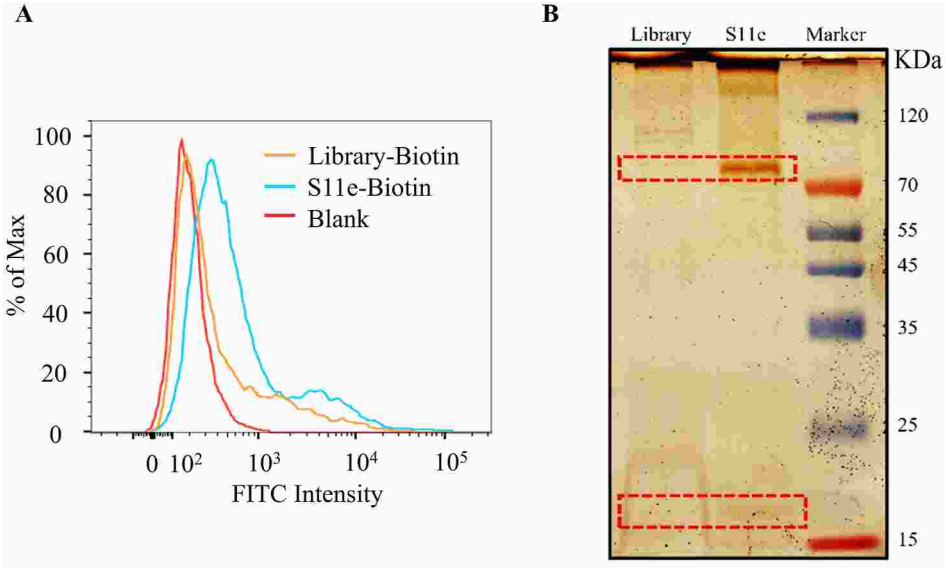

Fig. 9. S11e-binding proteins were analyzed by mass spectrometry. (A) The binding of biotin-modified S11e and Library to HT1080 cells was measured by flow cytometry. (B) Silver-stained SDS-PAGE was used to analyze aptamer target purification. Lane Library, protein captured with Library-treated sample; Lane S11e, protein captured with S11e-treated sample.

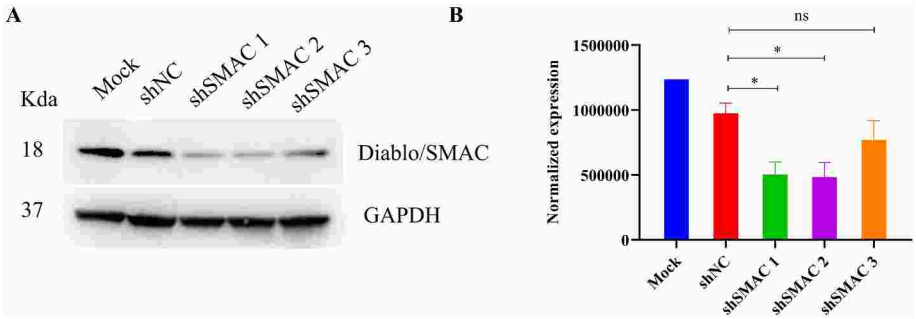

Fig. 10. Knockdown effects of Diablo/SMAC shRNAs. (A) HT1080 cells were infected with the indicated shRNAs. The infected cell extracts were analyzed using Western blotting with *anti*-Diablo/SMAC antibody. (B) Bar graph showing quantification of (A). (Comparison, shSMAC vs shNC: $*p < 0.05$; *ns*, not significant). NC: negative control.

results indicated that S11e can be internalized into HT1080 cells specifically.

In addition, we explored the internalization of S11e by colocalization analysis. Lysosome-tracker and Cy5-labeled S11e were co-incubated with HT1080 cells for 30 min, respectively, the fluorescent signals of lysosome-tracker and Cy5-labeled S11e were not overlapped (Fig. S5). After mitochondrial fluorescent probes Mito-tracker and Cy5-labeled S11e were used to co-incubate with HT1080 cells for 30 min, the fluorescent signals of Mito-tracker and Cy5-labeled S11e were partially overlapped. However, they are both completely overlapped for 1 h-incubation with HT1080 cells at 4 °C (Fig. 3C). We further test whether or not mitochondrial fluorescent probes are co-localized with Cy5-labeled S11e in MRC-5 cells. The results showed that only signals of mitochondrial fluorescent probes (green) were detected (Fig. S4), indicating no colocalization. Taken together, these results suggest that S11e can locate at the mitochondria in HT1080 cells. Our results also reveal that S11e can escape to mitochondria successfully without lysosomal internalization, making S11e an excellent potential carrier that can protect itself from degradation by various digestive enzymes in lysosomes.

3.4. *In vivo fluorescence imaging*

The ability of aptamers to recognize tumors *in vivo* is also important for clinical application. The stability of an aptamer affects its physiological condition, which is an important character to assess whether the aptamer can be clinically applied. However, when unmodified aptamers enter cells *in vivo*, they can be easily degraded by nucleases. Therefore, we modified oligonucleotides of aptamers to strengthen their resistance to nuclease degradation. Five bases at the 5′ end and five bases at the 3′ end of S11e and Library sequences were phosphorothioate modified. As shown in Fig. S6, the modified S11e sustained a relatively high concentration after 24 h in the blood serum. Then S11e was injected into mice *via* tail vein.

After the injection of S11e for 5 min, the fluorescence signal of S11e increased in the tumor sites, indicating that S11e aptamers accumulate rapidly in tumors. The fluorescence signal disappeared 2 h after injection, indicating that S11e can be excreted through kidney, liver and other metabolic organs (Fig. 4A). While after the injection of Library for 2 h, no obvious fluorescent signal was observed at the tumor sites, indicating that Library does not accumulate in tumors *in vivo*. The biological distribution of Cy5-labeled S11e and Cy5-labeled Library in mice was photographed 30 min after injection (Fig. 4B). Compared with the control group, mice injected with Cy5-labeled S11e showed accumulation of fluorescent signals in tumors. At the same time, fluorescent signals were observed in the kidney, liver, stomach and large intestine of the control group and the experimental group. Because of metabolism and rich of vessels, aptamers would induce some extent of wide distribution. These results suggest that S11e has the ability to target

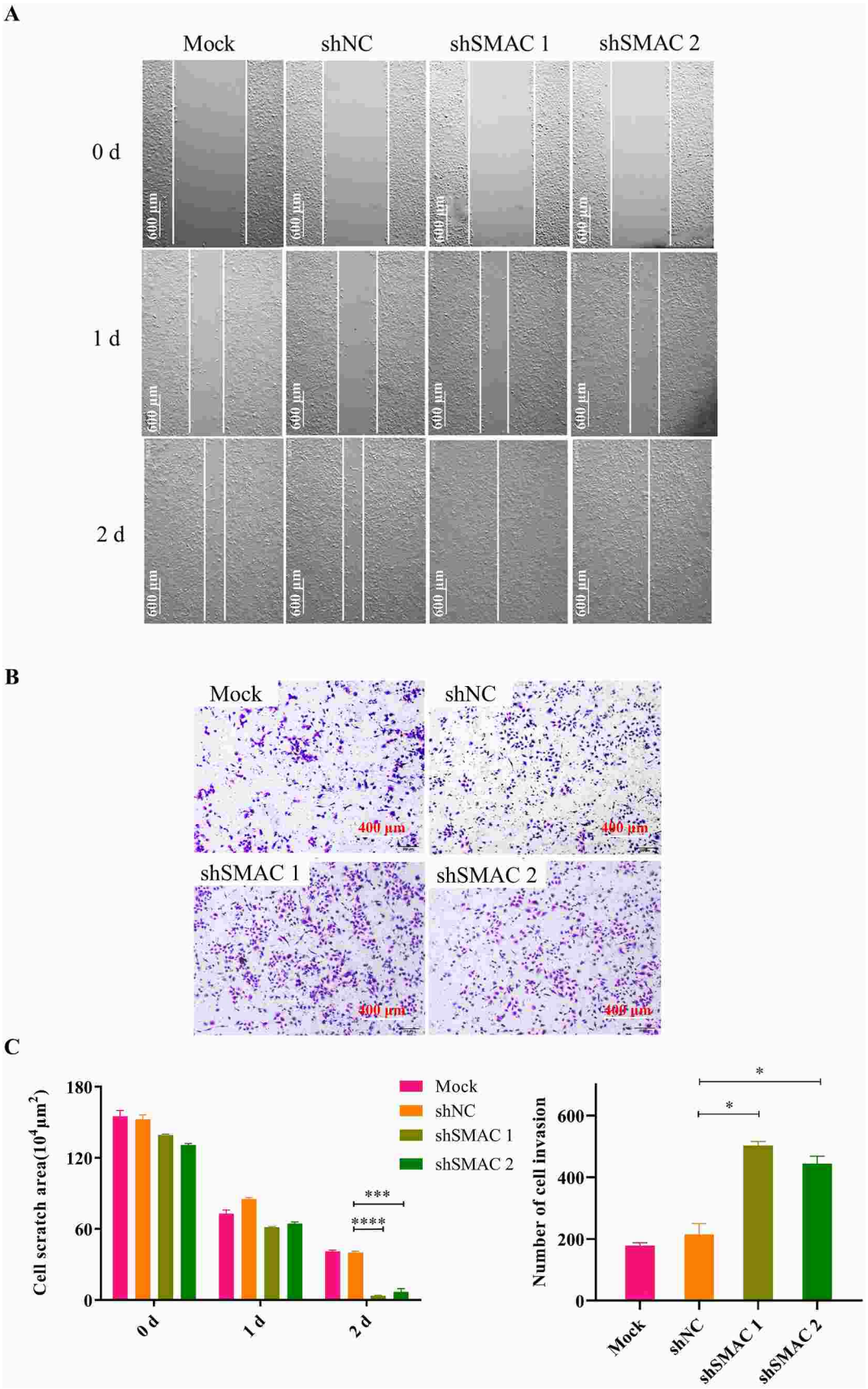

Fig. 11. Diablo/SMAC is identified as a functional target for S11e. After HT1080 cells were treated with the indicated shRNAs (shSMAC 1 and shSMAC 2), cell scratch test and invasion assay were conducted. The representative images of scratch test (A) and invasion assay (B) were shown. (C) Bar graphs showing quantification of triplicate results of A and B, respectively (Comparison, shSMAC vs shNC: $^{*}p < 0.05$; $^{**}p < 0.01$; $^{***}p < 0.001$; $^{****}p < 0.0001$). NC: negative control.

fibrosarcoma *in vivo*.

3.5. Imaging fibrosarcoma tissue array

Above experiments have shown that S11e is able to recognize HT1080 fibrosarcoma cells *in vivo* and *in vitro*. Next, we speculated that S11e could also recognize tumor tissues of fibrosarcoma. Cy5-labeled S11e and Cy5-labeled Library were incubated with fibrous histopathological slides, respectively. These slides contain 20 malignant fibrous histiocytoma tissues, 20 malignant fibrosarcoma tissues, 25 Dermatofibrosarcoma protuberances, 1 fibroxanthoma tissues, 4 myofibroma tissues, 4 fibrous histiocytoma tissues, 24 fibrous tissues, 4 fasciitis tissues and 2 normal tissues. The fluorescence results obtained by scanning with a Panoramic SCAN (3DHISTECH) are shown in Fig. 5. There was no red Cy5 fluorescence signal in normal tissues, while slight red fluorescence signal in benign cancer tissues and strong red fluorescence signal in malignant cancer tissues were observed. These results suggest that S11e can recognize fibrosarcoma tissue *in vitro*. Statistical analysis of fluorescence signals obtained from the combination of S11e and Library on tissue microarray were summarized in Table S3. This analysis reveals that S11e has little recognition ability to normal tissues, mild recognition ability to inflammatory tissues (25%), moderate recognition ability to benign cancer tissues (45%) and the strongest recognition ability to malignant cancer tissues (74%).

3.6. Biological function test

To investigate the biological function of S11e, cytotoxicity experiments were carried out. The 16 μM S11e and Library were added to HT1080 cells and treated for 24 h, 48 h and 72 h at 37 °C, respectively. After 24 h, the viability of HT1080 cells treated with S11e was lower than that of HT1080 cells treated with Library.

After 48 h, the viability of HT1080 cells in S11e group decreased by about 25% compared with that in Library group. The viability of HT1080 cells was 49.08% or 93.42% after treated with S11e or Library, respectively, suggesting that S11e but not Library has a cytotoxic effect on HT1080 cells (Fig. 6A).

As shown in Fig. 6B, the apoptosis was detected by flow cytometry using an Annexin V-FITC Apoptosis Detection Kit. The early apoptosis and late apoptosis ratios of HT1080 cells line treated with S11e increased to 9.08% and 9.79%, respectively, which were much higher than that of blank (0.443%, 0.00%) or Library (6.30, 1.01%). However, the early apoptosis and late apoptosis ratios of MRC-5 cells line treated with S11e were only 0.00% and 0.04%, respectively, which showed no significant difference compared with blank (0.00%, 0.07%) or Library (0.03%, 0.02%). Collectively, the results suggest that S11e effectively induces apoptosis in HT1080 cells indicating S11e′s potential therapeutic effect against tumor cells.

Next, we studied the pathway of S11e inducing apoptosis in HT1080 cells *via* Western blotting experiment. As shown in Fig. 7, the expression of cleaved-Caspase-9 (37 kDa), cleaved-Caspase-3 (17 kDa) and cleaved-PARP (89 kDa) increased in HT1080 cells after incubation with S11e. When Caspase-9 is activated, it activates Caspase-3, which further cleaves PARP, a key enzyme in apoptosis, and directly induces apoptosis. These results suggest that S11e specifically induces apoptosis through mitochondrial-mediated endogenous apoptotic pathway.

HT1080 is a highly metastatic cell line, which is often used in cell migration and invasion studies. We used scratch test to measure the effect of S11e on tumor cell migration. Scratches of HT1080 cells treated with medium healed completely at the second day. Scratches of HT1080 cells treated with Library healed 43% at the second day and almost healed completely at the third day. Scratches treated with S11e did not heal significantly even after 3 days (Fig. 8A). These results suggest that S11e significantly inhibits the migration of HT1080 cells (Fig. 8C).

We also conducted cell invasion test experiments (Fig. 8B). In HT1080 cells treated with S11e, the number of cells crossing the transwell chamber (363.5) was significantly lower than that in cells treated with culture medium (596.5) or Library (579.5), which proved that S11e could inhibit the invasion of HT1080 tumor cells (Fig. 8D).

3.7. Identification of S11e-binding protein through Mass Spectrometry Analysis

We next focused on the identification of functional cellular proteins that S11e binds to. HT1080 cells were incubated with S11e for 1 h. Total membrane proteins of HT1080 cells were extracted and incubated with biotin-labeled S11e or biotin-labeled Library, respectively. After analysis *via* flow cytometry assay, we first confirmed that biotin modification of S11e did not affect its binding to HT1080 cells (Fig. 9A). The binding complex was then separated by using streptavidin-coated agarose gel beads and analyzed through SDS-PAGE gel. Intriguingly, two protein bands with molecular weights of ~85 kDa and ~20 kDa were specifically detected in S11e treated cells, but not in Library-treated cells (Fig. 9B). The protein bands were then cut, trypsin digested and subjected to LC-MS/MS QSTAR analysis. The MS results showed a list of protein hits, which were shown in Table S4. Among these candidates, we focused on proteins with molecular weight between 15-25 kDa and 70–90 kDa, and then ranked them with the score ratio of S11e to Library. We found that Diablo/SMAC (21 kDa), which can be released from the mitochondrial intermembrane space to cytosol after an apoptotic trigger, ranked high compared to other hits. Therefore, we speculated Diablo/SMAC as a potential binding target of S11e.

To further confirm Diablo/SMAC is a functional binding target of S11e, we performed a loss-of-function analysis using three independent Diablo/SMAC-specific shRNAs. As shown in Fig. 10, shSMAC 1 and shSMAC 2 showed more significant knockdown effects on Diablo/SMAC compared to the control samples (Mock or negative control shRNA). We also conducted cell scratch test and invasion assay of SMAC silenced HT1080 cells treated with S11e (Fig. 11A and B). The results showed that the inhibition of cell migration and invasion in HT1080 cells by S11e was profoundly abolished in samples treated with shSMAC 1 and shSMAC 2. This result supports that SMAC is a functional binding target of S11e in fibrosarcoma cells.

4. Discussion

In this study, with a non-selective strategy using a known sequence pool of ssDNA aptamers, we identified that S11e, which was previously obtained by SELEX for NSCLC [26], can bind to fibrosarcoma HT1080 cells but not to human embryonic lung fibroblast MRC-5 cells. Also, S11e can recognize fibrosarcoma patient tissues *in vitro* and accumulate in the xenograft tumors in mice. Therefore, we report here an aptamer, i.e., S11e, that specifically recognizes fibrosarcoma.

Some aptamers are reported to be degraded by lysosome after entering the cytoplasm [28]. Interestingly, we found in this study that S11e located in mitochondria but not lysosome *via* fluorescence confocal microscopy imaging technique. We speculated that S11e may locate in mitochondria through ATP/ADP or other non-lysosomal transport pathways. It makes S11e a promising tool for targeting mitochondrial in cellular instead of conventional mitochondrial targeting strategies, which can protect the loading-drugs from being degraded by lysosomes [29]. However, the internalization mechanism of S11e still remains to be further studied.

In recent years, studies have shown that mitochondria play an important role in cell apoptosis [30]. When stimulated by apoptotic signals, mitochondria release cytochrome *c* into the cytoplasm and bind to Apaf-L to initiate the caspase cascade reaction. Cytochrome *c*/Apaf-1 complex activates caspase-9, which in turn activates caspase-3 to induce apoptosis [31]. We found that Caspase-9, Caspase-3 and PARP were cleaved in S11e-treated HT1080 cells *via* Western blotting analysis. Diablo/SMAC is closely related with apoptotic pathways in mitochondria [32], we hypothesize that Diablo/SMAC is involved in the apoptotic

function of S11e. However, Diablo/SMAC is immature in inner mitochondria and the mechanism that S11e induces apoptosis *via* Diablo/SMAC will be an intriguing question to be further studied.

Migration and invasion of malignant tumor cells is the obstacle for cancer treatment. The results of toxicity test and scratch test showed that S11e also could promote cell apoptosis and inhibit migration. Moreover, after Diablo/SMAC knockdown, the S11e inhibited migration and invasion was abolished. However, further studies may explore the correlation between Diablo/SMAC and migration-related pathways such as Akt pathway [33], which may provide new insights regarding the use of S11e as an effective prognostic tool in the clinical treatment of fibrosarcoma.

To sum up, the bio-functional aptamer with both *in vivo* and *in vitro* is rarely obtained by conventional cell-SELEX or protein-SELEX. Herein, we show that S11e exhibits high binding affinity and specificity to fibrosarcoma HT1080 cells. In addition, S11e is internalized into HT1080 cells independent of lysosome pathway and located in mitochondria. Furthermore, S11e promotes the apoptosis and inhibits the migration of HT1080 cells. Finally, we demonstrate that Diablo/SMAC protein is a biologically functional cellular target of S11e, suggesting that Diablo/SMAC is a potential therapeutic target for fibrosarcoma.

CRediT authorship contribution statement

Yunyi Liu: Investigation, Methodology, Formal analysis, Validation, Writing – original draft, Data curation. **Cheng Peng:** Investigation, Methodology, Formal analysis, Validation, Writing – original draft, Data curation. **Hui Zhang:** Investigation, Methodology, Software, Writing – review & editing. **Juan Li:** Investigation, Methodology, Software, Writing – review & editing. **Hailong Ou:** Investigation, Methodology, Software, Writing – review & editing. **Yang Sun:** Investigation, Methodology, Software, Writing – review & editing. **Chaoqi Wen:** Investigation, Methodology, Software, Writing – review & editing. **Dan Qi:** Formal analysis, Writing – original draft, Supervision, Writing – review & editing. **Xiaoxiao Hu:** Conceptualization, Resources, Data curation, Writing – original draft, Supervision, Writing – review & editing, Funding acquisition. **Erxi Wu:** Conceptualization, Resources, Data curation, Writing – original draft, Supervision, Writing – review & editing, Funding acquisition. **Weihong Tan:** Conceptualization, Resources, Data curation, Writing – original draft, Supervision, Writing – review & editing, Funding acquisition.

Declaration of competing interest

The authors have no competing interest to declare.

Acknowledgments

This work was supported by the National Natural Science Foundation of China (No. 31701249, 31970692, 81803068, 91953000, 21827811), Changsha Science and Technology Plan (kq2004009), Corbett Estate Fund for Cancer Research, the Hunan Provincial Key Area R&D Program (2019SK2201), Hunan Science and Technology Creative Program (2017XK2103), and the National Key R&D Program of China (2020YFA0909000). The authors would like to thank Euni Wu for the language editing of this manuscript.

Appendix A. Supplementary data

Supplementary data to this article can be found online at https://doi.org/10.1016/j.bioactmat.2021.10.011.

References

[1] M.D. Murphey, World Health Organization classification of bone and soft tissue tumors: modifications and implications for radiologists, Semin. Muscoskel. Radiol. 11 (2007) 201–214, https://doi.org/10.1055/s-2008-1038310.
[2] O. Meral, H. Uysal, Comparative proteomic analysis of fibrosarcoma and skin fibroblast cell lines, Tumour Biol 36 (2015) 561–567, https://doi.org/10.1007/s13277-014-2672-8.
[3] J.R. Toro, L.B. Travis, H.J. Wu, K. Zhu, C.D. Fletcher, S.S. Devesa, Incidence patterns of soft tissue sarcomas, regardless of primary site, in the surveillance, epidemiology and end results program, 1978-2001: an analysis of 26,758 cases, Int. J. Cancer 119 (2006) 2922–2930, https://doi.org/10.1002/ijc.22239.
[4] D. Augsburger, P.J. Nelson, T. Kalinski, A. Udelnow, T. Knösel, M. Hofstetter, J. W. Qin, Y. Wang, A.S. Gupta, S. Bonifatius, M. Li, C.J. Bruns, Y. Zhao, Current diagnostics and treatment of fibrosarcoma -perspectives for future therapeutic targets and strategies, Oncotarget 8 (2017) 104638–104653, https://doi.org/10.18632/oncotarget.20136.
[5] X. Wu, J. Chen, M. Wu, J.X. Zhao, Aptamers: active targeting ligands for cancer diagnosis and therapy, Theranostics 5 (2015) 322–344, https://doi.org/10.7150/thno.10257.
[6] L. Civit, S.M. Taghdisi, A. Jonczyk, S.K. Haßel, C. Gröber, M. Blank, H.J. Stunden, M. Beyer, J. Schultze, E. Latz, G. Mayer, Systematic evaluation of cell-SELEX enriched aptamers binding to breast cancer cells, Biochimie 145 (2018) 53–62, https://doi.org/10.1016/j.biochi.2017.10.007.
[7] H. Qu, A.T. Csordas, J. Wang, S.S. Oh, M.S. Eisenstein, H.T. Soh, Rapid and label-free strategy to isolate aptamers for metal ions, ACS Nano 10 (2016) 7558–7565, https://doi.org/10.1021/acsnano.6b02558.
[8] S.C. Gopinath, Y. Sakamaki, K. Kawasaki, P.K. Kumar, An efficient RNA aptamer against human influenza B virus hemagglutinin, J. Biochem. 139 (2006) 837–846, https://doi.org/10.1093/jb/mvj095.
[9] W. Xuan, Y. Xia, T. Li, L. Wang, Y. Liu, W. Tan, Molecular self-assembly of bioorthogonal aptamer-prodrug conjugate micelles for hydrogen peroxide and pH-independent cancer chemodynamic therapy, J. Am. Chem. Soc. 142 (2020) 937–944, https://doi.org/10.1021/jacs.9b10755.
[10] Y. Liu, H. Ou, X. Pei, B. Jiang, Y. Ma, N. Liu, C. Wen, C. Peng, X. Hu, Chemo-drug controlled-release strategies of nanocarrier in the development of cancer therapeutics, Curr. Med. Chem. (2020), https://doi.org/10.2174/0929867327666200605153919.
[11] G.J. Jaffe, D. Eliott, J.A. Wells, J.L. Prenner, A. Papp, S. Patel, A phase 1 study of intravitreous E10030 in combination with ranibizumab in neovascular age-related macular degeneration, Ophthalmology 123 (2016) 78–85, https://doi.org/10.1016/j.ophtha.2015.09.004.
[12] Y.H. Lao, K.K. Phua, K.W. Leong, Aptamer nanomedicine for cancer therapeutics: barriers and potential for translation, ACS Nano 9 (2015) 2235–2254, https://doi.org/10.1021/nn507494p.
[13] J.E. Rosenberg, R.M. Bambury, E.M. Van Allen, H.A. Drabkin, P.N. Lara Jr., A. L. Harzstark, N. Wagle, R.A. Figlin, G.W. Smith, L.A. Garraway, T. Choueiri, F. Erlandsson, D.A. Laber, A phase II trial of AS1411 (a novel nucleolin-targeted DNA aptamer) in metastatic renal cell carcinoma, Invest. N. Drugs 32 (2014) 178–187, https://doi.org/10.1007/s10637-013-0045-6.
[14] F. Schwoebel, L.T. van Eijk, D. Zboralski, S. Sell, K. Buchner, C. Maasch, W. G. Purschke, M. Humphrey, S. Zöllner, D. Eulberg, F. Morich, P. Pickkers, S. Klussmann, The effects of the anti-hepcidin Spiegelmer NOX-H94 on inflammation-induced anemia in cynomolgus monkeys, Blood 121 (2013) 2311–2315, https://doi.org/10.1182/blood-2012-09-456756.
[15] E. Leung, G. Landa, Update on current and future novel therapies for dry age-related macular degeneration, Expet Rev. Clin. Pharmacol. 6 (2013) 565–579, https://doi.org/10.1586/17512433.2013.829645.
[16] B. Jilma, P. Paulinska, P. Jilma-Stohlawetz, J.C. Gilbert, R. Hutabarat, P. Knöbl, A randomised pilot trial of the anti-von Willebrand factor aptamer ARC1779 in patients with type 2b von Willebrand disease, Thromb. Haemostasis 104 (2010) 563–570, https://doi.org/10.1160/th10-01-0027.
[17] Y. Morita, M. Leslie, H. Kameyama, D.E. Volk, T. Tanaka, Aptamer therapeutics in cancer: current and future, Cancers 10 (2018), https://doi.org/10.3390/cancers10030080.
[18] J. Hoellenriegel, D. Zboralski, C. Maasch, N.Y. Rosin, W.G. Wierda, M.J. Keating, A. Kruschinski, J.A. Burger, The Spiegelmer NOX-A12, a novel CXCL12 inhibitor, interferes with chronic lymphocytic leukemia cell motility and causes chemosensitization, Blood 123 (2014) 1032–1039, https://doi.org/10.1182/blood-2013-03-493924.
[19] R. Troisi, V. Napolitano, V. Spiridonova, I. Russo Krauss, F. Sica, Several structural motifs cooperate in determining the highly effective anti-thrombin activity of NU172 aptamer, Nucleic Acids Res. 46 (2018) 12177–12185, https://doi.org/10.1093/nar/gky990.
[20] E.W. Ng, D.T. Shima, P. Calias, E.T. Cunningham Jr., D.R. Guyer, A.P. Adamis, Pegaptanib, a targeted anti-VEGF aptamer for ocular vascular disease, Nat. Rev. Drug Discov. 5 (2006) 123–132, https://doi.org/10.1038/nrd1955.
[21] T. Watanabe, K. Hirano, A. Takahashi, K. Yamaguchi, M. Beppu, H. Fujiki, M. Suganuma, Nucleolin on the cell surface as a new molecular target for gastric cancer treatment, Biol. Pharm. Bull. 33 (2010) 796–803, https://doi.org/10.1248/bpb.33.796.
[22] S. Soundararajan, W. Chen, E.K. Spicer, N. Courtenay-Luck, D.J. Fernandes, The nucleolin targeting aptamer AS1411 destabilizes Bcl-2 messenger RNA in human breast cancer cells, Cancer Res. 68 (2008) 2358–2365, https://doi.org/10.1158/0008-5472.Can-07-5723.

[23] C. Maasch, K. Buchner, D. Eulberg, S. Vonhoff, S. Klussmann, Physicochemical stability of NOX-E36, a 40mer L-RNA (Spiegelmer) for therapeutic applications, Nucleic Acids Symp. Ser. (2008) 61–62, https://doi.org/10.1093/nass/nrn031.
[24] A.M. Verhagen, D.L. Vaux, Cell death regulation by the mammalian IAP antagonist Diablo/Smac, Apoptosis 7 (2002) 163–166, https://doi.org/10.1023/a:1014318615955.
[25] H. Zhang, Z. Wang, L. Xie, Y. Zhang, T. Deng, J. Li, J. Liu, W. Xiong, L. Zhang, L. Zhang, B. Peng, L. He, M. Ye, X. Hu, W. Tan, Molecular recognition and in-vitro-targeted inhibition of renal cell carcinoma using a DNA aptamer, Mol. Ther. Nucleic Acids 12 (2018) 758–768, https://doi.org/10.1016/j.omtn.2018.07.015.
[26] Z. Zhao, L. Xu, X. Shi, W. Tan, X. Fang, D. Shangguan, Recognition of subtype non-small cell lung cancer by DNA aptamers selected from living cells, Analyst 134 (2009) 1808–1814, https://doi.org/10.1039/b904476k.
[27] K.K. Karlsen, J. Wengel, Locked nucleic acid and aptamers, Nucleic Acid Therapeut. 22 (2012) 366–370, https://doi.org/10.1089/nat.2012.0382.
[28] W. Zhong, Y. Pu, W. Tan, J. Liu, J. Liao, B. Liu, K. Chen, B. Yu, Y. Hu, Y. Deng, J. Zhang, H. Liu, Identification and application of an aptamer targeting papillary thyroid carcinoma using tissue-SELEX, Anal. Chem. 91 (2019) 8289–8297, https://doi.org/10.1021/acs.analchem.9b01000.
[29] S. Fulda, L. Galluzzi, G. Kroemer, Targeting mitochondria for cancer therapy, Nat. Rev. Drug Discov. 9 (2010) 447–464, https://doi.org/10.1038/nrd3137.
[30] D.C. Chan, Mitochondria: dynamic organelles in disease, aging, and development, Cell 125 (2006) 1241–1252, https://doi.org/10.1016/j.cell.2006.06.010.
[31] Y.C. Su, J.L. Wu, J.R. Hong, Betanodavirus up-regulates chaperone GRP78 via ER stress: roles of GRP78 in viral replication and host mitochondria-mediated cell death, Apoptosis 16 (2011) 272–287, https://doi.org/10.1007/s10495-010-0565-x.
[32] V. Shoshan-Barmatz, N. Keinan, S. Abu-Hamad, D. Tyomkin, L. Aram, Apoptosis is regulated by the VDAC1 N-terminal region and by VDAC oligomerization: release of cytochrome c, AIF and Smac/Diablo, Biochim. Biophys. Acta 1797 (2010) 1281–1291, https://doi.org/10.1016/j.bbabio.2010.03.003.
[33] S. Goetze, A. Bungenstock, C. Czupalla, F. Eilers, P. Stawowy, U. Kintscher, C. Spencer-Hänsch, K. Graf, B. Nürnberg, R.E. Law, E. Fleck, M. Gräfe, Leptin induces endothelial cell migration through Akt, which is inhibited by PPARgamma-ligands, Hypertension 40 (2002) 748–754, https://doi.org/10.1161/01.hyp.0000035522.63647.d3.